第 36 卷第 2 期
2019 年 3 月

控 制 理 论 与 应 用
Control Theory & Applications

Vol. 36 No. 3
Mar. 2019

基于有效风速估计与预测的风电机组自适应最大风能跟踪控制

焦绪国[1], 杨秦敏[1†], 孙 勇[2], 应 有[2]

(1. 浙江大学 控制科学与工程学院 工业控制技术国家重点实验室, 浙江 杭州 310058;
2. 浙江运达风电股份有限公司, 浙江 杭州 310012)

摘要: 针对如何在有效风速未知情况下实现风电机组最大风能跟踪(MPPT)的问题, 本文使用支持向量回归(SVR)和自适应控制原理, 提出基于有效风速估计与预测的自适应MPPT控制方案. 首先, 使用机组的历史运行数据, 训练得到基于SVR的风速估计与预测模型, 为MPPT控制提供实时参考输入. 其次, 结合在线学习估计器(OLA)和减小转矩增益(DTG)控制原理, 设计自适应MPPT控制器, 该控制器能够较好应对系统未知动态特性和干扰, 且能降低传动链载荷. 最后, 使用李雅普诺夫原理证明闭环系统所有信号都是有界的. 仿真结果表明本文提出的方法能够获得良好的MPPT效果, 进而提高机组产能.

关键词: 最大风能跟踪器; 风电机组; 有效风速估计与预测; 自适应控制系统

引用格式: 焦绪国, 杨秦敏, 孙勇, 等. 基于有效风速估计与预测的风电机组自适应最大风能跟踪控制. 控制理论与应用, 2019, 36(3): 372 – 382

DOI: 10.7641/CTA.2018.80423

Adaptive maximum power point tracking control for wind turbines with effective wind speed estimation & prediction

JIAO Xu-guo[1], YANG Qin-min[1†], SUN Yong[2], YING You[2]

(1. State Key Laboratory of Industrial Control Technology, College of Control Science and Engineering, Zhejiang University, Hangzhou Zhejiang 310058, China;
2. Zhejiang Windey Co. Ltd., Hangzhou Zhejiang 310012, China)

Abstract: With the rapid development of wind power generation technology, maximum power point tracking (MPPT) control of wind turbines is still a challenging problem due to the unavailable effective wind speed. In this paper, an adaptive MPPT controller for wind turbines based on effective wind speed estimation & prediction is presented, without requiring the knowledge of system parameters, rotor or wind acceleration. Firstly, support vector regression (SVR) is utilized to develop the wind speed estimation & prediction models. The wind speed information is delivered to the MPPT controller in a real-time manner. Further, an online learning approximator (OLA) is employed in the controller to cope with the unknown dynamics of the wind turbines. Thus, the proposed OLA–based adaptive controller is parameter-free and can be readily extended to other types. Moreover, decreased torque gain control (DTG) is integrated to mitigate the mechanical loads on the driven train. Meanwhile, all signals in the closed-loop system are proven to be bounded via Lyapunov theory. Finally, the effectiveness of the proposed controller are validated with WP 1.5 MW wind turbines on the platform of FAST (Fatigue, Aerodynamics, Structures, and Turbulence) code and Simulink.

Key words: maximum power point trackers; wind turbines; effective wind speed estimation & prediction; adaptive control systems

Citation: JIAO Xuguo, YANG Qinmin, SUN Yong, et al. Adaptive maximum power point tracking control for wind turbines with effective wind speed estimation & prediction. *Control Theory & Applications*, 2019, 36(3): 372 – 382

1 Introduction

Development of renewable sources is considered to be the pivotal solution for the shortage of traditional energy and deterioration of environment. Owing to the relatively low cost of electricity generation[1], wind energy has become one of the promising renewable sources for the future and wind energy conversion system (WECS) has gained tremendous attention in recent years[2–4]. According to the wind market forecast report released by the international energy agency (IEA), global wind power penetration will be up to 15～18% by 2050[5].

Received 9 June 2018; accepted 25 December 2018.
†Corresponding author. E-mail: qmyang@zju.edu.cn; Tel.: +86 571-87952994.
Recommended by Associate Editor: JIA Hong-jie.
Supported by the National Natural Science Foundation of China (U1609214, 61673347, 61751205).

Due to the potential to extract maximum power from wind, variable-speed wind turbines (VSWT) dominate the market share in current wind power generation industry[6]. Researchers from control community have paid great attention to improve the power capture efficiency[2–3]. Tip speed ratio (TSR) based MPPT controllers have been widely recognized as a non-ideal, but practical solution in wind power generation industry[7]. It can convert the maximum power capture problem into an optimal rotor speed tracking task, provided that the effective wind speed information is available[3,6,8–11]. However, in practice, the traditional cup anemometer is installed behind the rotating rotor along the streamwise direction, and thus cannot provide accurate value of the effective wind speed. Therefore, how to obtain a satisfactory and low-cost estimate of wind speed has become the bottleneck problem for MPPT schemes.

In the recent decade, many researchers have shown their interests in effective wind speed estimation (EWSE) for VSWT's MPPT controller design. In the Kalman filter (KF) based EWSE approaches[4,12], the aerodynamic torque is regarded as an augmented system state, which is then estimated by the KF. The wind speed is thus derived from the explicit mathematical expression of the aerodynamic torque using an iterative algorithm, such as Newton's method. In the extended Kalman filter (EKF)[13–15] based EWSE methods, the nonlinear dynamics of wind speed is established firstly, and then the EKF algorithm is utilized to calculate effective wind speed value directly. Apparently, these approaches require the accurate mathematical model of VSWT or wind speed, which highly narrows their application in practice.

In order to get rid of the dependence on accurate system or wind speed models, machine learning algorithms based EWSE approaches have been presented in literature, which aim to build the nonlinear relationship between the output data of VSWT and effective wind speed. In [16], autoregressive statistical model is employed to estimate the wind speed, but the empirical two-dimentional look-up table of power coefficient and the power-mapping technique will occupy a lot of memory space and therefore reduce system performance[17]. A supervised artificial neural network (ANN) or support vector regression (SVR) is trained to build the relationship between the aerodynamic power, rotor speed and wind speed[17–19], but the construction of the training set requires a large amount of human intervention. In addition, to implement their EWSE strategies, rotor acceleration is required in calculating the aerodynamic power, which will increase the operation cost and introduce noise into the scheme[6]. Extreme learning machine (ELM) is also discussed in [20], but this methodology is only available for fixed-speed variable-pitch wind turbines. Moreover, all the existing EWSE approaches neglect the time delay introduced by the large inertia of VSWT which makes control system's response not instantaneous[19]. The low-pass filter introduced in the wind speed estimation model[21] also affects the accuracy of reference input and MPPT control performance.

In terms of EWSE based MPPT controller design, the proportional-integral (PI) schemes are proposed in [18] and [17], but these linear controllers fail to handle the nonlinearity or parameter uncertainties of VSWT satisfactorily. To take the nonlinear characteristics into consideration, nonlinear dynamic state feedback and sliding mode MPPT controllers are claimed in [4] and [22], respectively. However, they require the information of system parameters in the designed control signal, which will lead to deterioration of control performance when parameter drift happens. To deal with various unknown system parameters, neuroadaptive variable speed controller is designed for VSWT in [21], but the first and second time derivatives of the estimated wind speed, whose exact values are very difficult to attain, are required.

Therefore, in this paper, an effective wind speed estimation and prediction based MPPT controller for VSWT is developed, without using system parameters, rotor acceleration and time derivatives of estimated wind speed. First, a system model-free SVR based EWSE method is proposed. Certain output data of VSWT are collected to construct the training features for the SVR model, and a light detection and ranging (LIDAR) device is applied to acquire the accurate training targets (i.e., effective wind speed). Further, particle swarm optimization (PSO) algorithm is utilized to choose SVR parameters. By this means, the estimation accuracy can be improved without increasing the operation cost of the system. Second, based on the estimated wind speed series, an SVR based wind speed prediction approach is implemented. Compared with the estimated wind speed, the predicted wind speed is able to provide more reference information in advance, which is beneficial for the MPPT control performance. Further, by utilizing online learning approximator (OLA) to deal with the unknown dynamics of the system, a parameter-free adaptive controller is developed. The knowledge of exact value of rotor acceleration or time derivatives of estimated wind speed is relaxed. Moreover, decreased torque gain control (DTG) is integrated to mitigate the mechanical loads on driven train. Lyapunov theory based stability analysis guarantees the boundedness of all signals in the closed-loop system. Finally, simulations are conducted to validate the performance of the proposed approach.

The remainder of the paper is organized as follows. Section II presents a brief introduction of the VSWT's dynamics. In section III, the control objective is depicted in details. In section IV, the effective wind speed estimation and prediction technique is presented. Section V gives the detailed controller development methodology with stability analysis based on the Lyapunov theory. In Section VI, simulations with an 1.5 MW three-bladed VSWT are conducted. Finally, Section VII concludes the paper.

2 Dynamic model of VSWT

The dynamic model of the VSWT considered in this paper is shown in Fig. 1[8], which consists of wind rotor, driven train and generator subsystems. The aerodynamic power (rotor power) P_{a} captured by the wind turbine can be given as

$$P_{\mathrm{a}} = \frac{1}{2}\rho\pi R^2 C_{\mathrm{p}}(\lambda,\beta)v^3, \tag{1}$$

where ρ is the air density, R is the rotor swept radius, and v is the effective wind speed. The power coefficient C_{p} describes the capability of the turbine to harvest energy from wind. It is a nonlinear function of tip-speed ratio λ and pitch angle β. Generally, $C_{\mathrm{p}}(\lambda,\beta)$ is determined experimentally and provided by the manufacture. The following mathematical model can be utilized to approximate the power coefficient[23–24]

$$C_{\mathrm{p}}(\lambda,\beta) = \\ 0.5176(\frac{116}{\lambda_i} - 0.4\beta - 5)\mathrm{e}^{-\frac{21}{\lambda_i}} + 0.0068\lambda \tag{2}$$

with

$$\lambda_i = \frac{1}{\lambda + 0.08\beta} - \frac{0.035}{\beta^3 + 1}. \tag{3}$$

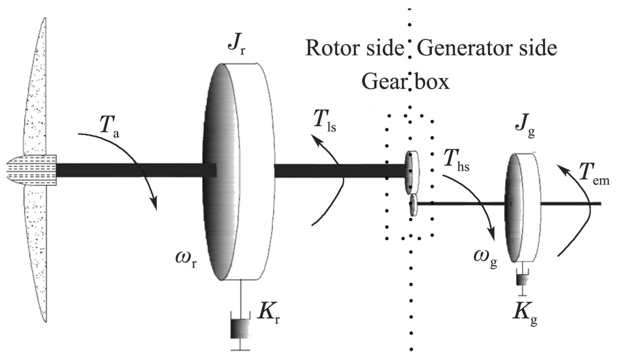

Fig. 1 Two-mass model of the VSWT

Figure 2 shows the power coefficient curves of the VSWT according to nonlinear functions (2) and (3). Each curve can be understood as the function of λ with a particular pitch angle β. It should be mentioned that C_{p} can take negative values when the wind turbine draws power from utility grid[6]. Further, λ is defined as the ratio of blade tip speed to wind speed upstream of the rotor

$$\lambda = \frac{R\omega_{\mathrm{r}}}{v} \tag{4}$$

with ω_{r} being the rotor speed. Meanwhile, using the basic physical law, P_{a} can be also calculated as

$$P_{\mathrm{a}} = T_{\mathrm{a}}\omega_{\mathrm{r}}, \tag{5}$$

where T_{a} is the aerodynamic torque obtained from the wind. Combining (1) and (5), one has

$$T_{\mathrm{a}} = \frac{1}{2}\rho\pi R^3 C_{\mathrm{q}}(\lambda,\beta)v^2 \tag{6}$$

with $C_{\mathrm{q}}(\lambda,\beta) = C_{\mathrm{p}}(\lambda,\beta)/\lambda$ the torque coefficient.

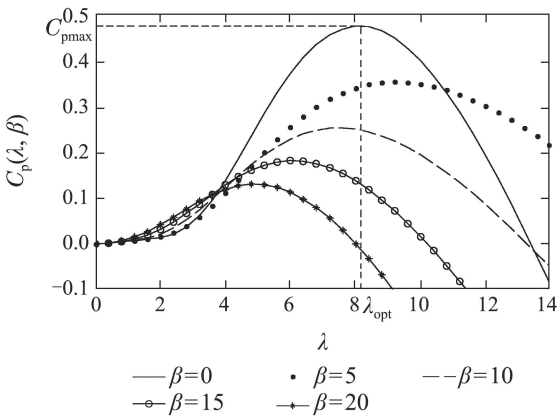

Fig. 2 Wind turbine power coefficient curves

Figure 1 shows the typical two-mass structure of VSWT. In the rotor side, the aerodynamic torque T_{a} drives the rotor inertia J_{r} at speed ω_{r} and braked by the low-speed shaft torque T_{ls}. In the generator side, the generator inertia J_{g} is driven by high-speed shaft torque T_{hs} at speed ω_{g} and the generator electromagnetic torque T_{em} acts as the braking torque on the generator. Therefore, the dynamics of the rotor and generator can be written as

$$J_{\mathrm{r}}\dot{\omega}_{\mathrm{r}} = T_{\mathrm{a}} - K_{\mathrm{r}}\omega_{\mathrm{r}} - T_{\mathrm{ls}}, \tag{7}$$

$$J_{\mathrm{g}}\dot{\omega}_{\mathrm{g}} = T_{\mathrm{hs}} - K_{\mathrm{g}}\omega_{\mathrm{g}} - T_{\mathrm{em}}, \tag{8}$$

where K_{r} and K_{g} are the external damping constants of rotor and generator, respectively. Moreover, a gear box is utilized to connect the low-speed shaft and high-speed shaft, and governs the ratio between ω_{r} and ω_{g} with the gearbox ratio n_{g} which can be defined as

$$n_{\mathrm{g}} = \frac{\omega_{\mathrm{g}}}{\omega_{\mathrm{r}}} = \frac{T_{\mathrm{ls}}}{T_{\mathrm{hs}}}. \tag{9}$$

By utilizing (7)–(9), the compact dynamic of VSWT can be further written as

$$\dot{\omega}_{\mathrm{r}} = \frac{1}{J_{\mathrm{t}}}(T_{\mathrm{a}} - K_{\mathrm{t}}\omega_{\mathrm{r}} - T_{\mathrm{g}}), \tag{10}$$

where

$$\begin{cases} J_{\mathrm{t}} = J_{\mathrm{r}} + n_{\mathrm{g}}^2 J_{\mathrm{g}}, \\ K_{\mathrm{t}} = K_{\mathrm{r}} + n_{\mathrm{g}}^2 K_{\mathrm{g}}, \\ T_{\mathrm{g}} = n_{\mathrm{g}} T_{\mathrm{em}} \end{cases} \tag{11}$$

are the lumped parameters.

VSWT always operates in highly turbulent and unpredicted environment[9,25], and severe external disturbances should be considered in controller design to improve the robustness of the control strategy. Thus, the following general dynamics of VSWT is studied

$$J_\mathrm{t}\dot{\omega}_\mathrm{r} = T_\mathrm{a} - K_\mathrm{t}\omega_\mathrm{r} - T_\mathrm{g} + d(t), \tag{12}$$

where $d(t)$ is the time-varying external disturbances.

Subsequently, (12) will be utilized for control analysis. Finally, the generator output power can be given as

$$P_\mathrm{g} = T_\mathrm{g}\omega_\mathrm{r}. \tag{13}$$

The following mild assumption is required in the subsequent development.

Assumption 1 The external disturbances $d(t)$ is upper bounded such that $|d(t)| \leqslant d_\mathrm{m}$, $\forall t > 0$ with $d_\mathrm{m} > 0$ being an unknown positive constant.

3 Problem formulation

VSWT can operate in three fundamental operation modes depending on the wind speed[8–9], which are illustrated in Fig. 3, where v_min, v_rated, and v_max are the cut-in, rated and cut-out wind speed, respectively. P_rated is the rated generator power. No wind power extraction occurs when the wind speed is below v_min. In Region 2, MPPT control is enforced to drive the turbine to extract energy from wind as much as possible, i.e., P_a should be maintained at its optimal value P_amax when the wind speed varies between v_min and v_rated. Moreover, the main controller task in Region 3 is to keep the generator power at its rated value to avoid over-speed and ensure the safety of the entire VSWT by altering the pitch angle β[8].

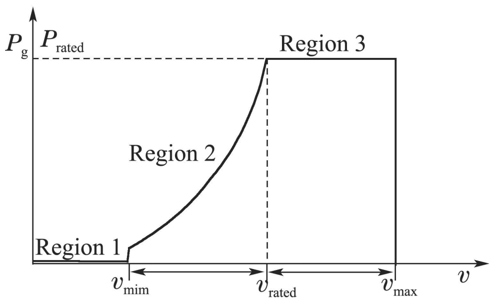

Fig. 3 Operating regions of VSWT

In this paper, the control task in Region 2 is considered. Using (1), the maximum power extraction value P_amax of the wind turbine can be defined as

$$P_\mathrm{amax} = \frac{1}{2}\rho\pi R^2 C_\mathrm{pmax}(\lambda, \beta)v^3, \tag{14}$$

where C_pmax is the optimal value of C_p. According to Fig. 1 and existing literature[8–9,21], the pitch angle β is always set as 0 and the system requires to be maintained at the optimal operation point λ_opt in order to capture the maximum power P_amax from wind. Recalling (4) implies that ω_r should be changed according to the wind speed to mach the optimum tip-speed ratio λ_opt, and hence the optimal rotor speed ω_ropt can be expressed as

$$\omega_\mathrm{ropt} = \frac{\lambda_\mathrm{opt}}{R}v. \tag{15}$$

However, in practice, the accurate information of the effective wind speed is still not accessible, and additional measurement equipment will also increase the overall cost of the wind turbine systems[22]. Therefore, let $\hat{\omega}_\mathrm{ropt}$ be the estimation of ω_ropt, and one has

$$\hat{\omega}_\mathrm{ropt} = \frac{\lambda_\mathrm{opt}}{R}\hat{v}, \tag{16}$$

where $\hat{v}$ is the predicted value of the actual wind speed v. Model (12) indicates that the equivalent generator electromagnetic torque T_g can be utilized to change the dynamics of the rotor speed. Therefore, the control objective of this study is to drive the rotor speed ω_r to track its estimated optimal value $\hat{\omega}_\mathrm{ropt}$ by designing an appropriate control law T_g. Firstly, define the tracking error as

$$e = \omega_\mathrm{r} - \hat{\omega}_\mathrm{ropt}. \tag{17}$$

Thus, the control objective is converted to eliminating the tracking error e. Because of the unavailable wind speed and unknown systematic parameters and dynamics, model (12) poses a challenging nonlinear uncertain control problem with unknown reference input and severe external disturbance.

Assumption 2 $\hat{\omega}_\mathrm{ropt}$ and its first time derivative $\dot{\hat{\omega}}_\mathrm{ropt}$ are upper bounded such that $|\hat{\omega}_\mathrm{ropt}(t)| \leqslant \omega_\mathrm{mr}$, $|\dot{\hat{\omega}}_\mathrm{ropt}(t)| \leqslant \omega_\mathrm{m}$, $\forall t > 0$ with ω_mr and $\omega_\mathrm{m} > 0$ being unknown positive constants.

4 Wind speed estimation and prediction

As stated above, MPPT control of VSWT requires the information of effective wind speed, which is defined as the spatial average of the wind field swept by the rotor and blades[11,22]. Generally in practice, wind speed is measured through mechanical cup anemometers, which are mounted on the top of the nacelle or on the wind-towers placed surrounding the wind turbines[11]. However, the anemometer can only measure wind speed at one point with large measurement error, which is not a good representative of the effective wind speed[18]. In order to improve the measurement accuracy, LIDAR based wind speed measurement technique is developed[6]. However, the price of LIDAR devices is comparatively high[6], which will increase the equipment and maintenance costs of wind farms. Therefore, from the perspective of control and reducing the cost of the overall VSWT system, it is of great significance to estimate the effective wind speed without involving additional hardware.

4.1 Support vector regression

SVR is widely used to tackle the regression tasks in machine learning. It can map the input features into a high-dimensional space, where the regression problem can be solved[26]. In particular, given a training set as

$$T_{\text{set}} = \{(x_1, y_1), \cdots, (x_l, y_l)\}, \tag{18}$$

where x_i and y_i, $i = 1, 2, \cdots, l$, are the input features and output targets, respectively. l is the number of training points. The SVR model can be defined as[26]

$$f(x) = w \cdot \psi(x) + b, \tag{19}$$

where w is the coefficient vector, x is the input vector, b is the bias term, and $\psi(\cdot)$ is a nonlinear function which maps x into a high-dimensional space.

The ε–SVR is applied in this paper to solve the following optimization problem

$$\min \frac{1}{2}\|w\|^2 + C\sum_{i=1}^{l}(\xi_i + \xi_i^*), \tag{20}$$

$$\text{s.t.} \begin{cases} y_i - w \cdot \psi(x_i) - b \leqslant \varepsilon + \xi_i^*, \\ w \cdot \psi(x_i) + b - y_i \leqslant \varepsilon + \xi_i, \\ \xi_i^*, \xi_i \geqslant 0, \end{cases} \tag{21}$$

where C determines the trade-off between the flatness of $f(\cdot)$ and the training errors of the model, ξ_i and ξ_i^* are slack variables, and ε is the parameter of insensitive loss function. Through solving the dual optimization problem of (20), the SVR model can be written as

$$f(x) = \sum_{i=1}^{l}(\alpha_i - \alpha_i^*)K(x, x_i) + b, \tag{22}$$

where α_i and α_i^* are Lagrange multipliers, $K(x, x_i)$ is the kernel function.

4.2 Wind speed estimation

In this subsection, SVR is implemented to obtain the nonlinear relationship between the output data of VSWT and the effective wind speed. The values of C and $K(x, x_i)$'s parameter have significant influence on the regression performance, and thus are optimized via PSO algorithm[27].

To obtain the effective wind estimation model, three output variables of the VSWT are selected: tower-top bearing fore-aft acceleration a_{fa}, blade 1 flapwise moment M_{yb1}, and blade 1 flapwise shear force F_{xb1}, i.e., $x_i = [a_{\text{fa}}\ M_{\text{yb1}}\ F_{\text{xb1}}]$. It should be noted that a_{fa} can be obtained through the existing supervisory control and data acquisition (SCADA) system. An accessible torque sensor is installed to measure M_{yb1}, and F_{xb1} can be calculated from M_{yb}. Therefore, the implementation of the proposed wind estimation method is practical in wind power generation industry. Since the number of samples is much larger than the number of features to be extracted, nonlinear kernel function is required to map the data into higher dimensional spaces[23]. In this study, the following nonlinear radial basis function (RBF)[23] is employed

$$K(x, x_i) = \exp(-\frac{\|x - x_i\|^2}{\varsigma^2}). \tag{23}$$

In the training phase of wind speed estimation model, LIDAR measurement is assumed to be available and thus the targets y_i, $i = 1, 2, \cdots, l$ of the training features x_i can be obtained. It should be noted that the LIDAR measurement device is only required in the training phase for a entire wind farm. After acquiring enough training data for wind speed estimation of one VSWT, the LIDAR device can be removed.

In order to prevent features in greater numeric ranges from dominating those in smaller ranges and improve the regression accuracy, the selected features are scaled to $[0, 1]$, by following

$$x_{i\_s} = \frac{x_i - \min(x_i)}{\max(x_i) - \min(x_i)}, \tag{24}$$

where x_{i_s} is the scaled features. $\min(x_i)$ and $\max(x_i)$ are the minimum and maximum values of original features x_i. Then the following low-pass filter is utilized to remove the high-frequency components of the estimated wind speed

$$G(s) = \frac{1}{\tau_0 s + 1}, \tag{25}$$

where $1/\tau_0$ is the bandwidth of the low-pass filter.

4.3 Wind speed prediction

On the other hand, the estimated wind speed possesses a time delay compared with the actual real-time wind speed. This delay occurs not only because the system response is not instantaneous due to the large inertia of the wind turbine[19], but also because the low-pass filter is employed in the wind speed estimation process. Thus, to improve the wind speed calculation accuracy and control performance, it is necessary to compensate the time delay by predicting the wind speed based on the estimated wind speed series.

In this paper, SVR is also utilized to build the wind speed prediction model. For clarity, SVR models used in wind speed estimation and prediction are labeled as SVR–I and SVR–II, respectively. The kernel function of SVR–II is chosen as RBF, and parameters C and ς^2 are determined by PSO algorithm as well. The targets y_i used in training SVR–I is employed to construct the training set of SVR–II. Let T be the sampling period of y_i, and the prediction interval is denoted by Δt. Then the training features Fea and targets Tar of SVR–II can be written as

$$Fea = \{y_i, y_{i+\Delta t/T}, y_{i+(2\Delta t)/T}, y_{i+(3\Delta t)/T}\}, \tag{26}$$

$$Tar = \{y_{i+(4\Delta t)/T}\},\ i = 1, 2, \cdots, l - (4\Delta t)/T \tag{27}$$

with l being the number of y_i.

The proposed wind speed estimation and prediction framework can be summarized as Fig. 4. In the offline training phase, effective wind speed estimation and prediction models can be obtained after training SVR–I and SVR–II. In the online implement phase, the scaled real-time turbine output data are inputted into the trained wind speed estimation model firstly. Then the designed low-pass filter is applied to smooth the wind speed estimation value. Finally, after inputting the estimated wind speed values into the trained wind speed prediction model, the predicted effective wind speed value is achieved.

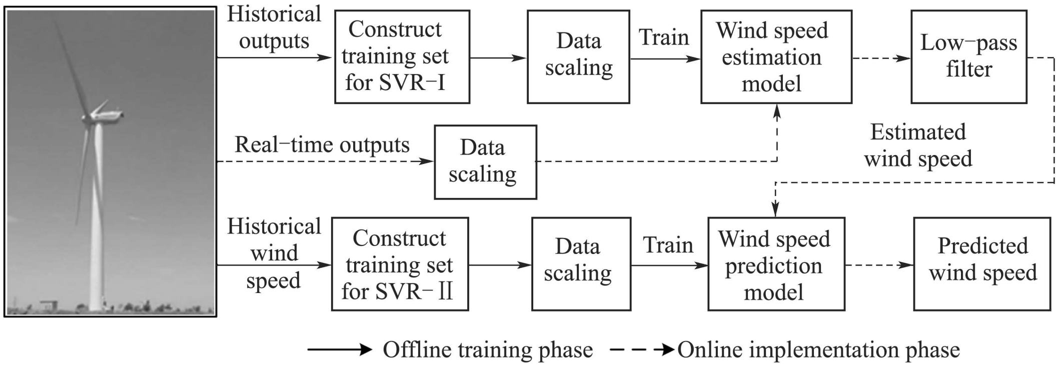

Fig. 4 Wind speed estimation and prediction framework

Thereafter, the relationship between the predicted effective wind speed and the actual wind speed is assumed to satisfy

$$\hat{v}(t) = v(t) + \zeta(t) \tag{28}$$

with $\zeta(t)$ the wind speed prediction error.

The following mild assumption is introduced before presenting the controller methodology.

Assumption 3 The wind speed prediction error $\zeta(t)$ is upper bounded such that $|\zeta(t)| \leqslant \zeta_{\mathrm{m}},\ \forall t > 0$ with $\zeta_{\mathrm{m}} > 0$ being an unknown positive constant.

5 Controller development

5.1 Dynamics of tracking error

By combining (6) and (28), the aerodynamic torque T_{a} can be rewritten as

$$\begin{aligned} T_{\mathrm{a}} = &\frac{1}{2}\rho\pi R^3 C_{\mathrm{q}}(\lambda,\beta)v^2 = \\ &\frac{1}{2}\rho\pi R^3 C_{\mathrm{q}}(\lambda,\beta)(\hat{v}-\zeta(t))^2 = \\ &\frac{1}{2}\rho\pi R^3 C_{\mathrm{q}}(\lambda,\beta)\hat{v}^2 - \rho\pi R^3 C_{\mathrm{q}}(\lambda,\beta)\hat{v}\zeta(t) + \\ &\frac{1}{2}\rho\pi R^3 C_{\mathrm{q}}(\lambda,\beta)\zeta^2(t). \end{aligned} \tag{29}$$

Moreover, according to (29) and Assumption 3 and considering the fact that $\beta = 0$ in Region 2 operation mode of VSWT, T_{a} can be represented as a function of ω_{r} and $\hat{v}$, plus a bounded disturbance $\delta(t)$[11]

$$T_a = \gamma(\omega_{\mathrm{r}}, \hat{v}) + \delta(t), \tag{30}$$

where $\delta(t)$ is bounded such that $|\delta(t)| \leqslant \delta_{\mathrm{m}}$ with δ_{m} being the unknown positive constant.

Further, combining (12) and (30), the dynamics of tracking error e can be expressed as

$$\begin{aligned} &J_{\mathrm{t}}\dot{e} = J_{\mathrm{t}}\dot{\omega}_{\mathrm{r}} - J_{\mathrm{t}}\dot{\hat{\omega}}_{\mathrm{ropt}} = \\ &T_{\mathrm{a}} - K_{\mathrm{t}}\omega_{\mathrm{r}} - T_{\mathrm{g}} + d(t) - J_{\mathrm{t}}\dot{\hat{\omega}}_{\mathrm{ropt}} = \\ &\gamma(\omega_{\mathrm{r}},\hat{v}) + \delta(t) - K_{\mathrm{t}}\omega_{\mathrm{r}} - T_{\mathrm{g}} + d(t) - J_{\mathrm{t}}\dot{\hat{\omega}}_{\mathrm{ropt}} = \\ &F(X) - T_{\mathrm{g}} + \delta(t) + d(t) - J_{\mathrm{t}}\dot{\hat{\omega}}_{\mathrm{ropt}}, \end{aligned} \tag{31}$$

where $F(X) = \gamma(\omega_{\mathrm{r}},\hat{v}) - K_{\mathrm{t}}\omega_{\mathrm{r}},\ X = [\omega_{\mathrm{r}},\hat{v}]$.

5.2 OLA and NN approximation

Notice that $F(X)$ is unknown due to the unknown function γ and unknown system parameters. Thus, in this paper, an OLA is utilized to approximate the unknown dynamics $F(X)$[28]. In particular, a two layer NN as shown in Fig. 5 is employed as as OLA. The output of the NN can be expressed as

$$O(A) = W^{\mathrm{T}}\phi(\Lambda^{\mathrm{T}}A), \tag{32}$$

where $A \in \mathbb{R}^{n_1}$ and $O \in \mathbb{R}^{n_2}$ are the input and output of NN, and n_1, n_2 and n_3 are the number of nodes in the input layer, hidden layer and output layer, respectively. The weights of hidden layer and output layer are denoted by $\Lambda \in \mathbb{R}^{n_1\times n_2}$ and $W \in \mathbb{R}^{n_2\times n_3}$, respectively. $\phi(\cdot) : \mathbb{R}^{n_2} \to \mathbb{R}^{n_2}$ is the activation function of the hidden layer. $\phi(\cdot)$ is chosen as the hyperbolic tangent sigmoid function[29] in this paper.

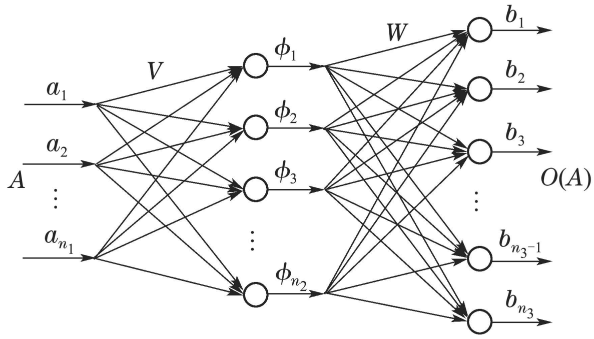

Fig. 5 Two layer NN structure

According to the universal NN approximation property[29], for all $A \in \mathbb{R}^{n_1}$ in a compact set Ω_A, any smooth function $G(A)$ can be written as

$$G(A) = W^{*\mathrm{T}}\phi(\Lambda^{\mathrm{T}}A) + \epsilon, \tag{33}$$

where W^* is the ideal weight of output layer, and ε

is the corresponding reconstruction error. It has been demonstrated that if the hidden layer weight Λ is chosen initially at random and held fixed subsequently, while n_2 is sufficiently large, the NN reconstruction error ϵ can be made arbitrarily small. Λ is omitted for convenience in the following context, because it is not updated in the learning process.

The following milda assumption can be commonly found in literature[6, 8, 29].

Assumption 4 The optimal weight W^* of NN and reconstruction error ϵ are upper bounded such that $\|W^*\| \leqslant W_{\rm m}$, $|\epsilon| \leqslant \epsilon_{\rm m}$, where $W_{\rm m}$ and $\epsilon_{\rm m}$ are unknown positive constants.

Notice that $F(X)$ is smooth function of rotor speed $\omega_{\rm r}$ and effective wind speed prediction value $\hat{v}$. Therefore, it can be approximated by an ideal NN as

$$F(X) = W^{*\rm T}\phi(X) + \epsilon, \tag{34}$$

where $X = [\omega_{\rm r}, \hat{v}]$. In practice, the optimal weight W^* is unavailable, and the estimation of W^* is denoted by $\hat{W}$.

Substituting (34) into (31) yields

$$\begin{aligned}&J_{\rm t}\dot{e} = \\ &W^{*\rm T}\phi(X) + \epsilon - T_{\rm g} + \delta(t) + d(t) - J_{\rm t}\dot{\hat{\omega}}_{\rm ropt} = \\ &W^{*\rm T}\phi(X) - T_{\rm g} + D(t),\end{aligned} \tag{35}$$

where $D(t) = \delta(t) + d(t) - J_{\rm t}\dot{\hat{\omega}}_{\rm ropt} + \epsilon$. According to Assumptions 1–2 and 4, one has

$$\begin{aligned}|D(t)| = &|\delta(t) + d(t) - J_{\rm t}\dot{\hat{\omega}}_{\rm ropt} + \epsilon| \leqslant \\ &\delta_{\rm m} + d_{\rm m} + J_{\rm t}\omega_{\rm m} + \epsilon_{\rm m} = D_{\rm m},\end{aligned} \tag{36}$$

where $D_{\rm m} = \delta_{\rm m} + d_{\rm m} + J_{\rm t}w_{\rm m} + \epsilon_{\rm m}$ is an unknown positive constant, and we denote the estimation of $D_{\rm m}$ by $\hat{D}_{\rm m}$.

5.3 Controller design

Based on the system dynamics (35), the control law can be given by

$$T_{\rm g} = ke + \hat{W}^{\rm T}\phi(X) + \hat{D}_{\rm m}{\rm sgn}\, e, \tag{37}$$

where $k > 0$ is the positive constant control gain. Note that there exists discontinuous signal sgn(·) in (37), which will bring chattering phenomena to control signal $T_{\rm g}$. In this paper, the continuous function tanh(·) is employed to replace sgn(·) to mitigate chattering phenomena. The following lemma reveals the numerical relationship between tanh(·) and sgn(·)[8].

Lemma 1 The following inequality holds for any $\eta \in \mathbb{R}$ and $\sigma > 0$

$$|\eta| - \eta\tanh\frac{\eta}{\sigma} \leqslant \kappa\sigma, \tag{38}$$

where $\kappa = 0.2758$.

Proof The proof is omitted here for simplicity. Please refer to [30] for details. QED.

Therefore, the proposed control law can be rewritten as

$$T_{\rm g} = ke + \hat{W}^{\rm T}\phi(X) + \hat{D}_{\rm m}\tanh\frac{e}{\sigma}. \tag{39}$$

Defining the updating law of $\hat{W}$ as

$$\dot{\hat{W}} = \Gamma(e\phi(X) - \sigma_1\hat{W}), \tag{40}$$

where $\Gamma = \Gamma^{\rm T} > 0$ is a positive definite symmetric matrix and $\sigma_1 > 0$ is a design constant. Further, the updating law of $\hat{D}_{\rm m}$ is chosen as

$$\dot{\hat{D}}_{\rm m} = \mu(e\tanh\frac{e}{\sigma} - \sigma_2\hat{D}_{\rm m}), \tag{41}$$

where $\mu > 0$ and $\sigma_2 > 0$ are positive constants designed by users. To reduce the change rate of the generator torque and mitigate the mechanical loads on driven train, the decreased torque gain (DTG) control[31] is introduced. Finally, the adaptive MPPT controller can be written as

$$T_{\rm g} = K_{\rm DTG}(ke + \hat{W}^{\rm T}\phi(X) + \hat{D}_{\rm m}\tanh\frac{e}{\sigma}) \tag{42}$$

with $0.8 \leqslant K_{\rm DTG} \leqslant 1$[31].

The diagram of the proposed MPPT controller is shown in Fig. 6. The wind speed estimation and prediction models provide effective wind speed value online and then the real-time estimated optimal rotor speed can be calculated. The stability of the proposed controller can be proven by the following theorem.

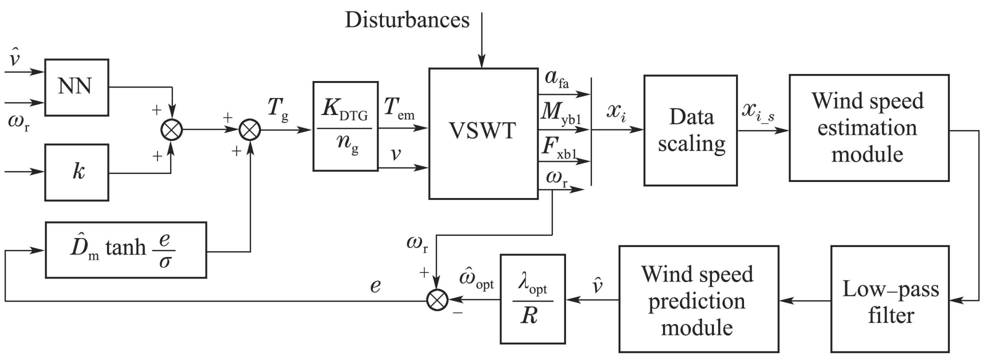

Fig. 6 Diagram of the proposed MPPT controller

Theorem 1 Consider the closed-loop system which consists of the rotor speed dynamics (12), the predicted desired rotor speed $\hat{\omega}_{\mathrm{ropt}}$, and the NN adaptive controller (42) with the updating rule (40) and (41), the tracking error e and all the other signals are bounded.

Proof Please see Appendix A.

6 Verification studies

To demonstrate the effectiveness of the proposed method, it is implemented with the FAST (fatigue, aerodynamics, structures, and turbulence) code, which is developed by NREL (national renewable energy laboratory) and extensively utilized by wind power technology developers in academia and industries[6,8,10]. The WP 1.5 MW wind turbine[25] model is employed in the simulation, and its main parameters are shown in Table 1.

Table 1 Main parameters of wind turbine model

Number of blades	3
Rotor radius	35 m
Hub height	84.288 m
Gear box ratio	87.965
Rated power	1.5 MW
Cut-in wind speed	3 m/s
Rated wind speed	12 m/s
Cut-out wind speed	1.5 m/s
Rotor inertia	2.962×10^6 kg · m^2
Generator inertia	53.036 kg · m^2
λ_{opt}	7.0
C_{pmax}	0.412

Note that the external disturbance $d(t)$ is considered in the controller development. In order to test the robustness of the proposed control approach, the term "CompNoise" is set as "True" in the FAST's input file. This means that six different forms of aerodynamic noise including turbulent inflow, turbulent boundary layer trailing edge, separating flow, laminar boundary layer vortex shedding, trailing edge bluntness vortex shedding, and tip vortex formation are superimposed by a series of semi-empirical noise calculation algorithms, and then the total noise are added into the dynamics of wind turbines[25].

6.1 Results of effective wind speed estimation and prediction

To acquire the training data for effective wind speed estimation and prediction models, LIDAR wind speed measurement device, whose measurement precision is very high[6], is supposed to be installed on the VSWT. After getting enough training data for SVR–I and SVR–II, the LIDAR device can be removed to other wind turbines in the wind farm. Therefore, we only need one LIDAR device to build wind speed estimation and prediction models for every wind turbine of the entire wind farm. The dataset obtained from wind turbine system can be seperated into two parts: one is used as the training set and the other is employed as testing set. Fig. 7 shows the training data for EWSE model, including historical effective wind speed v, tower-top bearing fore-aft acceleration a_{fa}, blade 1 flapwise moment M_{yb1} and blade 1 flapwise shear force F_{xb1}.

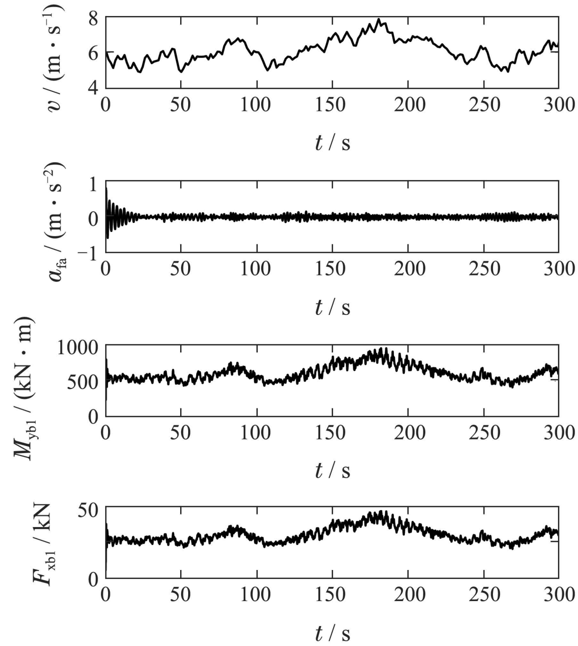

Fig. 7 Training data for effective wind speed estimation model

In the offline training phase, the training process of wind speed estimation and prediction models is implemented with LIBSVM[32] software package. PSO algorithm is used to seek the important parameters C and ς^2 of SVR. In PSO algorithm, the number of evaluation generations and the population size are set as 200 and 20, respectively. For SVR–I, the optimal C and ς^2 are found to be 80.0774 and 2.3299, respectively. Meanwhile, for SVR–II, C and ς^2 are optimized as 10.0324 and 0.5687, respectively.

The turbulent wind profile used in the simulation is generated by TurbSim[21]. The mean wind speed is set as 6 m/s, and the turbulence intensity is chosen as 13%. The estimated wind speed and real wind speed in the offline test phase are shown in Fig. 8. The mean-squared error (MSE) between the estimated wind speed and the real wind speed is 0.0487, and the mean absolute percent error (MAPE) of them is 2.9290%.

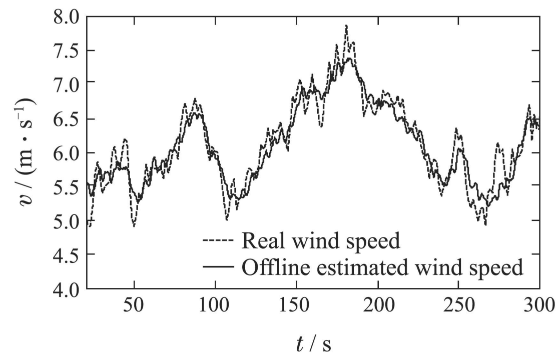

Fig. 8 Offline wind speed estimation performance comparison

In the online implementation phase, the predicted wind speed, estimated wind speed and real wind speed are compared in Fig. 9. The MSE and MAPE between the estimated wind speed and the real wind speed are 0.0698 and 3.3926%, respectively, while the MSE and MAPE between the predicted wind speed and the real wind speed are 0.0695 and 3.3884%, respectively. This indicates that the wind speed calculation accuracy is improved through prediction operation.

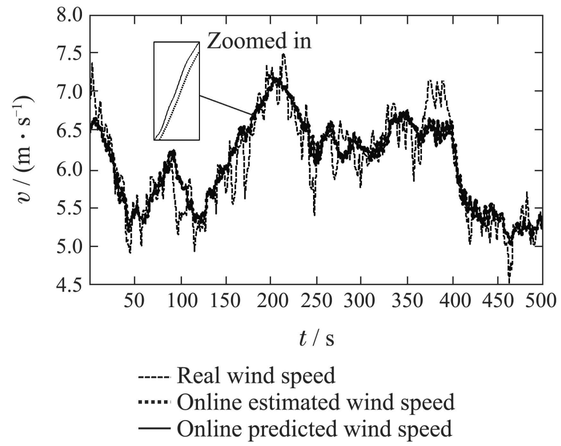

Fig. 9 Online wind speed estimation and prediction performance comparison

The proposed wind speed estimation algorithm is compared with the NN–based wind speed estimation method in [17]. Fig.10 shows the wind speed estimation comparison results of NN–based in [17] and the proposed method. The MSE and MAPE of the NN–based method in [17] is 0.1580 and 5.3648%, respectively, which indicates that the proposed wind speed estimation algorithm can achieve better performance.

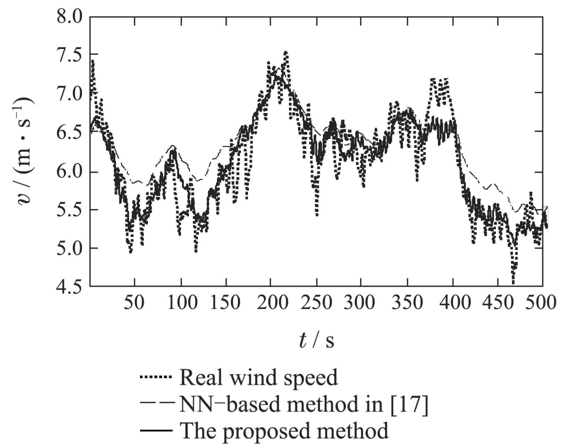

Fig. 10 Comparison results of the two wind speed estimation approaches

6.2 Tracking performance of the proposed MPPT controller

In this subsection, the tracking performance of the proposed EWSE and prediction based MPPT controller is verified. In our validation, the parameters are set as follows: air density $\rho = 1.225\,\mathrm{kg/m^3}$, optimal tip-speed ratio $\lambda_{\rm opt} = 7.0$, $C_{\rm pmax} = 0.412$[8,10]. Furthermore, the controller parameters are tuned as: $n_2 = 8$, $k = 7\times 10^6$, $\Gamma = \mathrm{diag}\{10^5, \cdots, 10^5\}$, $\sigma = 10^{-2}$, $\sigma_1 = 5\times 10^{-7}$, $\sigma_2 = 10^{-5}$, $\mu = 10^5$, $\tau_0 = 2$, $\Delta t = 2\,\mathrm{s}$. It should be noted that these parameters are utilized in both offline training phase and online implementation phase.

We compare the proposed controller with the following standard optimal torque controller (OTC)[10] and a well-tuned PI controller with NN–based wind speed estimator given by[17]

$$T_{\rm gOTC} = k_{\rm opt}\omega_{\rm r}^2, \tag{43}$$

$$T_{\rm gPI} = K_{\rm P}e + K_{\rm I}\int e(t)\mathrm{d}t, \tag{44}$$

where $k_{\rm opt} = 0.5\rho\pi R^5 C_{\rm pmax}/\lambda_{\rm opt}^3$, $K_{\rm P} = 8\times 10^5$, $K_{\rm I} = 6\times 10^4$.

The rotor speed tracking performance is shown in Fig. 11 and Fig. 12. The MSE of optimal rotor speed tracking errors of OTC control, PI control in [17] and the proposed algorithm are 1.1572, 0.5310 and 0.2972, respectively, which indicates the proposed method can achieve better tracking performance with smaller tracking error than the traditional OTC and PI control in [17]. The resulting generator torque and output power are depicted in Fig. 13 and Fig. 14, respectively.

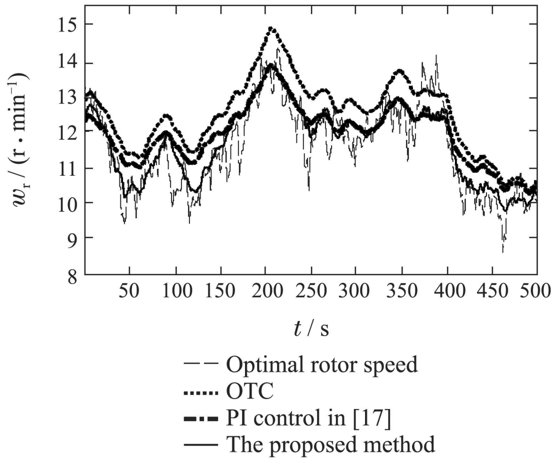

Fig. 11 Rotor speed tracking performance

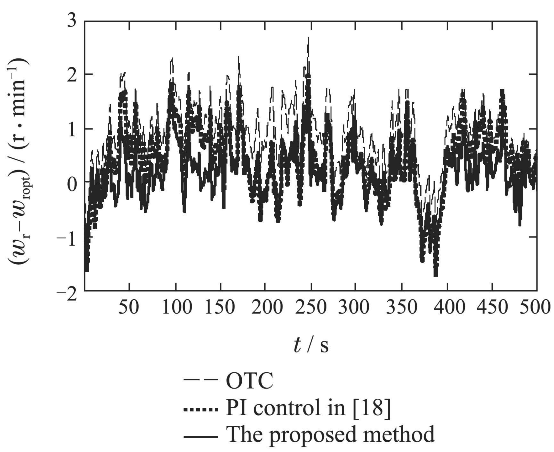

Fig. 12 Resulting rotor speed tracking errors

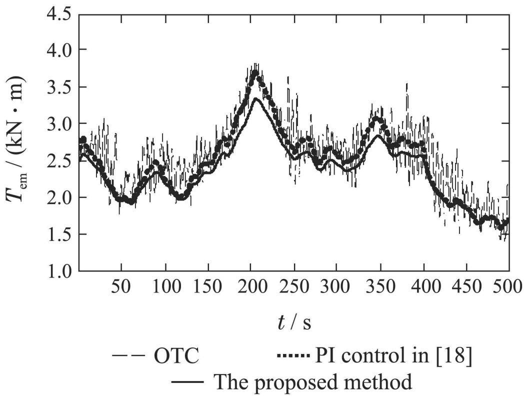

Fig. 13 Resulting generator torques

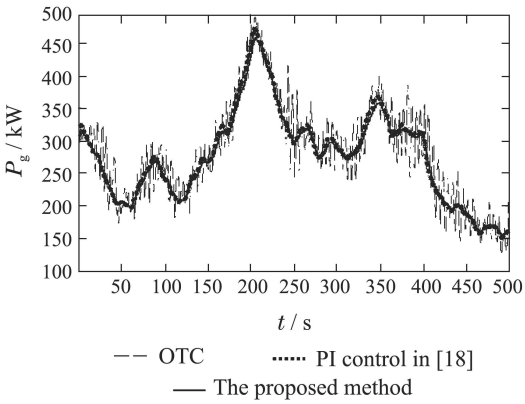

Fig. 14 Resulting generator powers

The total generation over the simulation time is 39.1278 $\mathrm{kW \cdot h}$ when only the wind speed estimation model is used, while the total generation can be improved to 39.1444 $\mathrm{kW \cdot h}$ after using both wind speed estimation and prediction models, which demonstrates the effectiveness of the proposed wind speed prediction method. Compared with the generation of 38.1807 $\mathrm{kW \cdot h}$ generated by OTC and 38.5083 $\mathrm{kW \cdot h}$ generated by PI scheme, the amount of generation is increased by 2.524% and 1.652% with the proposed MPPT approach, respectively. Therefore, by utilizing the proposed MPPT controller, the economic efficiency of wind farms can be improved significantly.

7 Conclusions

In this paper, effective wind speed estimation and prediction based MPPT control of VSWT is investigated. First, a model-free SVR based EWSE technique is developed and PSO algorithm is utilized to choose the important SVR parameters. The input of the wind speed estimation model are tower-top bearing fore-aft acceleration, blade 1 flapwise moment and blade 1 flapwise shear force. These variables can be obtained through the existing SCADA system and a cheap torque sensor, thus the proposed wind estimation method's implementation cost is low. Second, to improve the MPPT control performance, an SVR based wind speed prediction model is developed to provide reference input in advance, compared with the estimated wind speed. Moreover, by combining two-layer NN and adaptive control algorithm, the parameter-free MPPT controller is designed. The rotor and wind acceleration information is not required in the proposed controller, thus its implementation cost is low. In addition, DTG is introduced to mitigate the mechanical loads of the driven train. Rigid stability analysis shows that all the signals in the closed-loop system are bounded. The experimental results on FAST/Simulink shows the proposed control scheme can predict the effective wind speed with high accuracy and achieve excellent MPPT tracking performance.

References:

[1] JAIN T, YAMÉ J J, SAUTER D D. A novel trajectory-based online controller design approach to fault accommodation in NREL' s 5 MW wind turbine systems. *Control Theory and Technology*, 2014, 12(2): 122 – 131.

[2] KUMAR D, CHATTERJEE K. A review of conventional and advanced MPPT algorithms for wind energy systems. *Renewable and Sustainable Energy Reviews*, 2016, 55: 957 – 970.

[3] ABDULLAH M A, YATIM A H M, TAN C W, et al. A review of maximum power point tracking algorithms for wind energy systems [J]. *Renewable and Sustainable Energy Reviews*, 2012, 16(5): 3220 – 3227.

[4] BOUKHEZZAR B, SIGUERDIDJANE H. Nonlinear control of a variable-speed wind turbine using a two-mass model. *IEEE Transactions on Energy Conversion*, 2014, 29(2): 418 – 425.

[5] MARAYANA M, SUNDERLAND K M, PUTRUS G, et al. Adaptive Linear Prediction for Optimal Control of Wind Turbines. *Renewable Energy*, 2017, 113: 895 – 906.

[6] SHE Y, SHE X, BARAN M E. Universal tracking control of wind conversion system for purpose of maximum power acquisition under hierarchical control structure. *IEEE Transactions on Energy Conversion*, 2011, 26(3): 766 – 775.

[7] KNIGHT A M, PETERS G E. Simple wind energy controller for an expanded operating range. *IEEE Transactions on Energy Conversion*, 2005, 20(2): 459 – 466.

[8] MENG W, YANG Q, YINH Y, et al. Adaptive power capture control of variable-speed wind energy conversion systems with guaranteed transient and steady-state performance. *IEEE Transactions on Energy Conversion*, 2013, 28(3): 716 – 725.

[9] BAGHERIEH O, NAGAMUNE R. Gain-scheduling control of a floating offshore wind turbine above rated wind speed. *Control Theory and Technology*, 2015, 13(2): 160 – 172.

[10] IYASERE E, SALAH M H, DAWSO D M H, et al. Robust nonlinear control strategy to maximize energy capture in a variable speed wind turbine with an internal induction generator. *Journal of Control Theory and Applications*, 2012, 10(2): 184 – 194.

[11] MENG W, YANG Q, SUN Y. Guaranteed performance control of DFIG variable-speed wind turbines. *IEEE Transactions on Control Systems Technology*, 2016, 24(6): 2215 – 2223.

[12] KANELLOS F D, HATZIARGYRIOU N D. Optimal control of variable speed wind turbines in islanded mode of operation. *IEEE Transactions on Energy Conversion*, 2010, 25(4): 1142 – 1151.

[13] SOLTANI M N, KNUDSEN T, SVENSTRUP M, et al. Estimation of rotor effective wind speed: A comparison. *IEEE Transactions on Control Systems Technology*, 2013, 21(4): 1155 – 1167.

[14] SONG D, YANG J, DONG M, et al. Kalman filter-based wind speed estimation for wind turbine control. *International Journal of Control, Automation and Systems*, 2017, 15(3): 1 – 8.

[15] SONG D, YANG J, CAI Z, et al. Wind estimation with a non-standard extended Kalman filter and its application on maximum power extraction for variable speed wind turbines. *Applied Energy*, 2017, 190: 670 – 685.

[16] TAN K, ISLAM S. Optimum control strategies in energy conversion of PMSG wind turbine system without mechanical sensors. *IEEE Transactions on Energy Conversion*, 2004, 19(2): 392 – 399.

[17] QIAO W, ZHOU W, ALLER J. Wind speed estimation based sensorless output maximization control for a wind turbine driving a DFIG. *IEEE Transactions on Power Electronics*, 2008, 23(3): 1156 – 1169.

[18] LI H, SHI K L, MCLAREN P G. Neural-network-based sensorless maximum wind energy capture with compensated power coefficient. *IEEE Transactions on Industry Applications*, 2005, 41(6): 1548 – 1556.

[19] ABO-KHALIL A G, AHMED G, LEE D. MPPT control of wind generation systems based on estimated wind speed using SVR. *IEEE Transactions on Industrial Electronics*, 2008, 55(3): 1489 – 1490.

[20] WU S, WANG Y, CHENG S. Extreme learning machine based wind speed estimation and sensorless control for wind turbine power generation system. *Neurocomputing*, 2013, 102: 163 – 175.

[21] LI D, CAI W, LI P, et al. Neuroadaptive variable speed control of wind turbine with wind speed estimation. *IEEE Transactions on Industrial Electronics*, 2016, 63(12): 7754 – 7764.

[22] JENA D, RAJENDRAN S. A review of estimation of effective wind speed based control of wind turbines. *Renewable and Sustainable Energy Reviews*, 2015, 43: 1046–1062.

[23] MOZAYAN S M, SAAD M, VAHEDI H, et al. Sliding mode control of PMSG wind turbine based on enhanced exponential reaching law. *IEEE Transactions on Industrial Electronics*, 2016, 63(10): 6148 – 6159.

[24] MUHANDO E. B, SENJYU T U, TOMONOBU U A, et al. LQG design for megawatt-class WECS with DFIG based on functional models' fidelity prerequisites. *IEEE Transactions on Energy Conversion*, 2009, 24(4): 893 – 904

[25] JONKMAN J M, BUHL Jr M L. *Fast user's guide-updated august 2005* [R]. Golden, CO, United States: National Renewable Energy Lab, 2005.

[26] SMOLA A J, SCHÖLKOPF B. A tutorial on support vector regression. *Statistics and Computing*, 2004, 14(3): 199 – 222.

[27] LIN S W, YING K C, CHEN S C. Particle swarm optimization for parameter determination and feature selection of support vector machines. *Expert Systems with Applications*, 2008, 35(4): 1817 – 1824.

[28] FAN B, YANG Q, JAGANNATHAN S, et al. Asymtotic tracking controller design for nonlinear systems with guaranteed performance. *IEEE Transactions on Cybernetics*, 2017.

[29] YANG Q, JAGANNATHAN S, SUN Y. Robust integral of neural network and error sign control of MIMO nonlinear systems. *IEEE Transactions on Neural Networks and Learning Systems*, 2015, 26(12): 3278 – 3286.

[30] CHEN M, GE S S, REN B. Adaptive tracking control of uncertain MIMO nonlinear systems with input constraints. *Automatica*, 2011, 47(3): 452 – 465.

[31] JOHNSON K E, FINGERSH L J, BALAS M J, et al. Methods for increasing region 2 power capture on a variable-speed wind turbine. *Journal of solar energy engineering*, 2004, 126(4): 1092 – 1100.

[32] CHANG C C, LIN C J. LIBSVM: a library for support vector machines. *ACM Transactions on Intelligent Systems and Technology*, 2011, 2(3): 27.

Appendix Proof of Theorem 1

Proof Consider the following Lyapunov function

$$V = \frac{J_{\mathrm{t}}}{2}e^2 + \frac{1}{2K_{\mathrm{DTG}}}\tilde{W}^{\mathrm{T}}\varGamma^{-1}\tilde{W} + \frac{1}{2lK_{\mathrm{DTG}}}\tilde{D}_{\mathrm{m}}^2, \quad \text{(A1)}$$

where $\tilde{W} = W^* - K_{\mathrm{DTG}}\hat{W},\ \tilde{D}_{\mathrm{m}} = D_{\mathrm{m}} - K_{\mathrm{DTG}}\hat{D}_{\mathrm{m}}$. Taking its time derivative and recalling (35)(39)–(41), we have

$$\begin{aligned}&\dot{V} = \\ &eJ_{\mathrm{t}}\dot{e} - \tilde{W}^{\mathrm{T}}\varGamma^{-1}\dot{\tilde{W}} - \frac{1}{l}\tilde{D}_{\mathrm{m}}\dot{\tilde{D}}_{\mathrm{m}} = \\ &e(-K_{\mathrm{DTG}}ke + \tilde{W}^{\mathrm{T}}\phi(X) - K_{\mathrm{DTG}}\hat{D}_{\mathrm{m}}\tanh\frac{e}{\sigma} + \\ &D(t)) - \tilde{W}^{\mathrm{T}}(e\phi(X) - \sigma_1\hat{W}) - \tilde{D}_{\mathrm{m}}(e\tanh\frac{e}{\sigma} - \sigma_2\hat{D}_{\mathrm{m}}) \leqslant \\ &-K_{\mathrm{DTG}}ke^2 + e\tilde{W}^{\mathrm{T}}\phi(X) - eK_{\mathrm{DTG}}\hat{D}_{\mathrm{m}}\tanh\frac{e}{\sigma} + \\ &|e|D_{\mathrm{m}} - \tilde{W}^{\mathrm{T}}(e\phi(X) - \sigma_1\hat{W}) - \tilde{D}_{\mathrm{m}}(e\tanh\frac{e}{\sigma} - \sigma_2\hat{D}_{\mathrm{m}}).\end{aligned} \quad \text{(A2)}$$

Utilizing inequality (38) further gives

$$\begin{aligned}&\dot{V} \leqslant \\ &-K_{\mathrm{DTG}}ke^2 + e\tilde{W}^{\mathrm{T}}\phi(X) - eK_{\mathrm{DTG}}\tilde{D}_{\mathrm{m}}\tanh\frac{e}{\sigma} + \\ &\kappa\sigma D_{\mathrm{m}} - \tilde{W}^{\mathrm{T}}(e\phi(X) - \sigma_1\hat{W}) - \tilde{D}_{\mathrm{m}}(e\tanh\frac{e}{\sigma} - \sigma_2\hat{D}_{\mathrm{m}}) \leqslant \\ &-K_{\mathrm{DTG}}ke^2 + \kappa\sigma D_{\mathrm{m}} + \frac{\sigma_1}{K_{\mathrm{DTG}}}\tilde{W}^{\mathrm{T}}(W^* - \tilde{W}) + \\ &\frac{\sigma_2}{K_{\mathrm{DTG}}}\tilde{D}_{\mathrm{m}}(D_{\mathrm{m}} - \tilde{D}_{\mathrm{m}}).\end{aligned} \quad \text{(A3)}$$

By applying the Young's inequality to (A3), there is

$$\begin{aligned}\dot{V} \leqslant\ &-K_{\mathrm{DTG}}ke^2 + \kappa\sigma D_{\mathrm{m}} - \frac{\sigma_1}{K_{\mathrm{DTG}}}\|\tilde{W}\|^2 + \\ &\frac{\sigma_1}{2K_{\mathrm{DTG}}}\|\tilde{W}\|^2 + \frac{\sigma_2}{K_{\mathrm{DTG}}}W_{\mathrm{m}}^2 - \frac{\sigma_2}{2K_{\mathrm{DTG}}}|\tilde{D}_{\mathrm{m}}|^2 + \\ &\frac{\sigma_2}{2K_{\mathrm{DTG}}}|\tilde{D}_{\mathrm{m}}|^2 + \frac{\sigma_2}{2K_{\mathrm{DTG}}}D_{\mathrm{m}}^2 = \\ &-K_{\mathrm{DTG}}ke^2 - \frac{\sigma_1}{2K_{\mathrm{DTG}}}\|\tilde{W}\|^2 - \frac{\sigma_2}{2K_{\mathrm{DTG}}}|\tilde{D}_{\mathrm{m}}|^2 + \\ &\kappa\sigma D_{\mathrm{m}} + \frac{\sigma_1}{2}W_{\mathrm{m}}^2 + \frac{\sigma_2}{2K_{\mathrm{DTG}}}D_{\mathrm{m}}^2 \leqslant \\ &-c_1V(t) + c_2,\end{aligned} \quad \text{(A4)}$$

where $c_1 = \min(2K_{\mathrm{DTG}}/J_{\mathrm{t}}, \sigma_1/\gamma_{\max}(\varGamma), \sigma_2 l) > 0,\ c_2 = \kappa\sigma D_{\mathrm{m}} + (\sigma_1/(2K_{\mathrm{DTG}}))W_{\mathrm{m}}^2 + (\sigma_2/(2K_{\mathrm{DTG}}))D_{\mathrm{m}}^2 > 0$.

Further, considering the following differential equation

$$\frac{\mathrm{d}(V\mathrm{e}^{c_1t})}{\mathrm{d}t} = c_1V\mathrm{e}^{c_1t} + \dot{V}\mathrm{e}^{c_1t}. \quad \text{(A5)}$$

Combining (A4) and (A5), one has

$$\frac{\mathrm{d}(V\mathrm{e}^{c_1t})}{\mathrm{d}t} \leqslant c_1V\mathrm{e}^{c_1t} + (-c_1V(t) + c_2)\mathrm{e}^{c_1t} \leqslant c_2\mathrm{e}^{c_1t}. \quad \text{(A6)}$$

Then, integrating both sides of (A6) with the initial value $V(0)$ gives

$$V\mathrm{e}^{c_1t} - V(0) \leqslant \frac{c_2}{c_1}\mathrm{e}^{c_1t} - \frac{c_2}{c_1}. \quad \text{(A7)}$$

Moreover, (A7) can be rewritten as

$$0 \leqslant V(t) \leqslant V(0)\mathrm{e}^{-c_1t} + \frac{c_2}{c_1}(1 - \mathrm{e}^{-c_1t}),\ \forall t \geqslant 0. \quad \text{(A8)}$$

Therefore, e, $\tilde{W}$ and $\tilde{D}_{\mathrm{m}}$ are bounded. Since $\hat{W} = W^* - K_{\mathrm{DTG}}\tilde{W}$ and $\hat{D}_{\mathrm{m}} = D_{\mathrm{m}} - K_{\mathrm{DTG}}\tilde{D}_{\mathrm{m}}$, and D_{m} and W^* are bounded by definition, one has that $\hat{W}$ and $\hat{D}_{\mathrm{m}}$ are bounded. From (39) and (11), T_{g} and T_{em} are bounded. According to (17) and Assumption 2, ω_{r} is bounded. Recalling (9), ω_{g} is also bounded. Moreover, (13) indicates the boundness of P_{g}. The boundness nature of v guarantees the boundness of T_{a}. Recalling the boundness of T_{g}, we can conclude that the tower-top bearing fore-aft acceleration a_{fa} is bounded according to the basic physical law. Therefore, all the signals in the closed-loop system are bounded. QED.

作者简介:

焦绪国 博士研究生, 目前研究方向为风力发电系统与自适应控制, E-mail: xuguojiao@zju.edu.cn;

杨秦敏 博士, 教授, 博士生导师，目前研究方向为智能电网与可再生能源、智能控制系统理论、工业大数据与人工智能, E-mail: qmyang@zju.edu.cn;

孙　勇 硕士, 目前研究方向为风电机组控制技术, E-mail: suny@chinawindey.com;

应　有 硕士, 目前研究方向为风电机组控制技术, E-mail: yingy@chinawindey.com.